Cerebral Cortex, 2017; 1–12

doi: 10.1093/cercor/bhx029
Original Article

ORIGINAL ARTICLE

β-Catenin in the Adult Visual Cortex Regulates NMDA-Receptor Function and Visual Responses

M. Hadi Saiepour[1], Rogier Min[1], Willem Kamphuis[1], J. Alexander Heimel[1] and Christiaan N. Levelt[1,2]

[1]Department of Molecular Visual Plasticity, Netherlands Institute for Neuroscience, Royal Netherlands Academy of Arts and Science, Meibergdreef 47, 1105 BA Amsterdam, the Netherlands and [2]Department of Molecular and Cellular Neurobiology, Center for Neurogenomics and Cognitive Research, VU University Amsterdam, de Boelelaan 1085, 1081 HV Amsterdam, the Netherlands

Address correspondence to Christiaan N. Levelt. Email: c.levelt@nin.knaw.nl

Abstract

The formation, plasticity and maintenance of synaptic connections is regulated by molecular and electrical signals. β-Catenin is an important protein in these events and regulates cadherin-mediated cell adhesion and the recruitment of pre- and postsynaptic proteins in an activity-dependent fashion. Mutations in the β-catenin gene can cause cognitive disability and autism, with life-long consequences. Understanding its synaptic function may thus be relevant for the treatment of these disorders. So far, β-catenin's function has been studied predominantly in cell culture and during development but knowledge on its function in adulthood is limited. Here, we show that ablating β-catenin in excitatory neurons of the adult visual cortex does not cause the same synaptic deficits previously observed during development. Instead, it reduces NMDA-receptor currents and impairs visual processing. We conclude that β-catenin remains important for adult cortical function but through different mechanisms than during development.

Key words: contrast sensitivity, NMDA-receptor, ocular dominance plasticity, synaptic, visual cortex

Introduction

Calcium-dependent cell adhesion through the N-cadherin–β-catenin complex has been identified as an important factor in synapse morphology and plasticity during forebrain development, and interfering with this complex during development has a severe impact on synaptic transmission (Tang et al. 1998; Bozdagi et al. 2000; Goda 2002; Murase et al. 2002; Togashi et al. 2002; Bamji et al. 2003; Bozdagi et al. 2004; Okamura et al. 2004; Nuriya and Huganir 2006; Okuda et al. 2007; Tai et al. 2007; Vitureira et al. 2012). This contribution of β-catenin to brain development and synaptic function gained additional interest in recent years because mutations in the β-catenin gene were found to cause intellectual disability (Tucci et al. 2014) and autism spectrum disorders (ASDs) (O'Roak et al. 2012; Krumm et al. 2014), and changes in the regulation of β-catenin stability by glycogen synthase kinase 3β (GSK3β) have been implicated in schizophrenia (Mao et al. 2009; Chen et al. 2015). In addition, the antidepressant lithium increases β-catenin stability (Beaulieu et al. 2009) and antipsychotics such as clozapine, haloperidol, or risperidone increase β-catenin expression in the rat medial prefrontal cortex and striatum (Alimohamad et al. 2005). Together, these findings identify β-catenin as potential link between the pathogenesis and treatment of these brain disorders.

During synapse formation and plasticity, N-cadherin distribution at the synapse is regulated by interactions with its major binding partner β-catenin. β-Catenin links N-cadherin to the actin cytoskeleton through interactions with α-catenin (Ozawa et al. 1989; Drees et al. 2005; Yamada et al. 2005) and recruits additional proteins to the synapse (Brigidi and Bamji 2011). The interaction of N-cadherin with β-catenin is strengthened by

synaptic activity (Murase et al. 2002; Schuman and Murase 2003; Tai et al. 2007). Presynaptically, this increases the clustering of synaptic vesicles (Murase et al. 2002; Bamji et al. 2003), while postsynaptically, it recruits the postsynaptic scaffold protein PSD95 and the AMPA receptor (AMPAR) GluA2 subunit to the synapse (Murase et al. 2002; Okuda et al. 2007). These pre- and postsynaptic molecular modifications are paralleled by reduced synaptic depression and increased synaptic efficacy, respectively (Bamji et al. 2003; Okuda et al. 2007; Vitureira et al. 2012). As part of the canonical Wnt-signaling pathway, β-catenin also acts as a transcriptional co-factor for TCF/LEF family of transcription factors (Barker et al. 2000). NMDA-receptor (NMDAR) activation in hippocampal neurons was found to result in nuclear translocation of β-catenin and increased TCF/LEF-dependent gene expression (Abe and Takeichi 2007).

Most studies on the role of β-catenin have been performed in the developing brain or by using neuronal cell cultures. This is highly relevant, as the mental disorders in which β-catenin is implicated start during brain development. On the other hand, these disorders last beyond development and antipsychotics and antidepressant drugs are used in adulthood. We therefore studied the synaptic function of β-catenin in the adult cortex. Using the primary visual cortex (V1) as a model, we asked whether cortical function or plasticity are affected when the β-catenin gene is disrupted. We provide evidence that in the absence of β-catenin, AMPAR-mediated synaptic transmission in excitatory cortical neurons in V1 is not altered, while NMDAR/AMPAR ratios are reduced. While reduced NMDAR expression did not affect plasticity in adult V1, it did cause deterioration of visual processing. These findings suggest that β-catenin has different functions at different stages of brain maturation which may have important implications for the pathogenesis and treatment of neurodevelopmental disorders in which β-catenin function is affected.

Materials and Methods

Animals

For this study, we made use of homozygous conditional β-catenin-deficient mice (Junghans et al. 2005) also carrying the G35-3 cre transgene. The G35-3 cre transgene is expressed in excitatory neurons of the cortex and hippocampus efficiently starting during early adulthood (Sawtell et al. 2003; Chakravarthy et al. 2006). Littermates negative for the G35-3 cre transgene but homozygous for the targeted β-catenin locus were used as controls for all experiments. Both the conditional β-catenin-deficient mouse line and the G35-3 cre line were backcrossed to C57BL/6J background for at least 6 generations. To ensure that deletion of the conditional β-catenin locus was complete, all the experiments were done in mice which were older than 4 months of age. Mice were housed in 12 h light–dark conditions and had access to food and water ad libitum. All experiments were approved by the institutional animal care and use committee of the Royal Netherlands Academy of Arts and Sciences.

Tissue Preparation and Synaptic Membrane Isolation

Protein extracts enriched for synaptic membranes were prepared from binocular V1. The procedure is explained in detail in Dahlhaus et al. (2011). Dissected binocular cortices were snap-frozen in liquid nitrogen, and stored at −80 °C. They were homogenized in ice-cold homogenization buffer (0.32 M sucrose in 5 mM HEPES and EDTA-free protease inhibitor [Roche] at pH 7.4), and centrifuged at 1000 × *g* for 10 min at 4 °C to precipitate cellular debris. Supernatant was loaded on a sucrose column consisting of 1.2 and 0.85 M sucrose. After ultracentrifugation at 110 000 × *g* for 2 h at 4 °C, the fraction at the interface of 0.85 and 1.2 M sucrose, containing the synaptosomes was collected. An osmotic shock of synaptosomes by a hypotonic HEPES solution resulted in their lysis, after which they were run on another sucrose column (0.85 and 1.2 M) and ultracentrifugation at 70 000 × *g* for 30 min at 4 °C. Synaptic membranes were collected from the phase border of the two sucrose concentrations. Protein concentrations were determined using a micro BCA protein assay kit (Thermoscientific).

Western Blotting

Extracted synaptic membranes were used for western blotting. For every antibody, a gradient of concentration of proteins, between 1 and 6 µg, was separately examined to achieve an easily detectable signal which had a relatively linear relationship to the concentration of loaded proteins. All materials were purchased from Invitrogen. Based on NuPage protocol (Invitrogen) proteins were treated with sodium dodecyl sulfate (SDS) and reduced at 70 °C and loaded on a NuPAGE 4–12% continuous Bis-Tris gel (Invitrogen). Transfer of proteins was done overnight (14 V, at 4 °C) to an Immobilon-P PVDF (Polyvinylidene Difluoride) paper (Immobilon-FL, Millipore) that was already activated by 100% methanol and soaked in transfer buffer containing 0.1% antioxidant. To increase the retention of transferred proteins, PVDF papers were dried after being washed and then kept at −20 °C for storage. Staining the membranes was done after reactivation of membranes by 100% methanol, and subsequent washes with distilled water and TBS (Tris-buffered saline). The papers were blocked with 1% casein in TBS for 45 min and were incubated with primary antibodies, dissolved in 0.3% casein solution in TBST (Tris-buffered saline, 0.1% Triton), for an hour at room temperature. Primary antibodies that were used are as follows: mouse-anti-β-catenin, α-catenin, γ-catenin, and N-cadherin (α-catenin 1:500, the others 1:2000, Transduction Laboratories), mouse anti NMDAR2A/B (1:1000, Chemicon) and rabbit anti S-SCAM (1:250, Sigma). Papers were then washed with TBST and incubated for 1 h at room temperature with infrared IRDye®800CW-labeled secondary antibodies (goat-α-mouse-IR [926–32210] and/or goat-α-rabbit-IR [926–32211], LI-COR Biosciences; 1:5000) in TBST with 0.01% SDS. Papers were washed 3 times with TBST and then with TBS, after which they were scanned using the Odyssey® Infrared Imager (LI-COR Biosciences). Fluorescence intensities of IR secondary antibodies were quantified using the Odyssey 2.1 software package (LI-COR Biosciences). Western blotting data were compared by Student's *t*-test (2-tailed, independent samples).

Slice Electrophysiology

Mice (>4 months old) were anesthetized by intraperitoneal (i.p.) injection of sodium pentobarbital (40 mg/kg) and perfused with 5 mL ice-cold choline chloride-based artificial cerebrospinal fluid (ACSF). After decapitation, brains were chilled in ice-cold carbogenated (95% O_2/5% CO_2) choline cloride-based ACSF, containing 110 mM choline chloride, 7 mM $MgCl_2$, 0.5 mM $CaCl_2$, 2.5 mM KCl, 11.6 mM Na-ascorbate, 3.10 mM Na-pyruvate, 1.25 NaH_2PO_4, 25 mM D-glucose, and 25 mM $NaHCO_3$ (Bureau et al. 2006). We prepared 330-µm coronal slices of V1 using a vibrating microtome (ThermoFisher Scientific). Slices were stored in submerged chambers containing carbogenated normal ACSF comprising 125 mM NaCl, 3 mM KCl, 2 mM $MgSO_4$, 2 mM $CaCl_2$, 10 mM glucose,

1.20 mM NaH_2PO_4 and 26 mM $NaHCO_3$ (305 mOsm and pH 7.3) for half an hour at 36 °C and later at room temperature. For miniature excitatory postsynaptic currents (mEPSCs), borosilicate glass patch-pipettes (3–4 MΩ) were filled with K-gluconate internal solution containing 110 mM K-gluconate, 10 mM KCl, 10 mM Hepes, 4 mM MgATP, 10 mM K_2phosphocreatine, 0.3 mM GTP. The pH was set to 7.3 and osmolarity to 290 mOsm. The recordings were done at 32 ± 0.5 °C under an Axioskop FS upright microscope equipped with infrared Hoffman modulation contrast optics (Zeiss) and VX 45 infrared camera (Optronis). Recordings were done blind to genotype.

Analysis of mEPSCs

Mini analysis (Synaptosoft, Inc.) was used for analyzing mEPSCs. The amplitude threshold was set at 9 pA, which was >3× root-mean-square noise in all recordings. After automatic detection of mEPSCs by the software, each mEPSC was visually inspected. Recordings with a systematic drift in average mEPSC rise time of >10% were excluded. mEPSCs with rise times >3 ms were omitted.

AMPA/NMDA Ratios

For recording AMPA/NMDA ratios, L2/3 pyramidal neurons were patched with intracellular solution containing (mM): 120 $CsMeSO_3$, 8 NaCl, 15 $CsCl_2$, 10 TEA-Cl, 10 HEPES, 2 QX-314, 4 MgATP, 0.3 Na_2GTP (pH 7.3). The extracellular solution contained (mM): 125 NaCl, 2.5 KCl, 1.25 NaH_2PO_4, 25 $NaHCO_3$, 1 $MgCl_2$, 2 $CaCl_2$, and 25 glucose. GABAzine (1 μM) was added to the extracellular solution to block $GABA_A$ receptors, and glycine (10 μM) was added to saturate the NMDAR co-agonist binding site. EPSCs were evoked by extracellular stimulation using a monopolar stimulating pipette positioned 50–100 μm next to the soma of the recorded neuron. Stimulation position and strength (~20 μA for 0.2 ms) were adjusted to obtain an evoked EPSC with a smooth rise and decay. Then, EPSCs were recorded every 10 s with the neuron alternating between a holding potential of −80 and +40 mV. For analysis, 10–20 EPSCs at each holding potential were averaged. The size of the AMPA component was defined as the peak amplitude of the EPSC recorded at −80 mV, while the NMDA component was defined as the response 30 ms later at +40 mV.

White Matter Stimulation

Input/output (I/O) curves were measured by stimulation of white matter (with a bipolar electrode with the poles 160 μm apart) and recording in both layer 4 and layer 2/3. The recording electrodes were placed in a way that a minimum response could be detected by a 15 μA stimulus (20 μs). Stimulus intensity was increased with increments of 30 μA until a maximal response could be reached. For each stimulus intensity, 6 repetitions were done, which were averaged and analyzed.

Paired-Pulse Ratio and Stimulus Trains

Paired-pulse ratio was measured when half maximal stimuli (20 μs) were repetitively applied (40 Hz). The responses were recorded 20 times and averaged for analysis. The size of second peak to the first was considered as paired-pulse ratio. To run down the docked pool of vesicles 80 pulses (14 Hz) were applied for 20 times with 30 s intervals. The averages of last 5 response peaks were compared with the first 5.

Immunohistochemistry

After anesthesia with i.p. injection of pentobarbital (40 mg/kg weight), mice were perfused with 5 mL of 1× phosphate-buffered saline (PBS) and then 50 ml of 4% PFA (Sigma) in PBS. Brains were post-fixed in 4% PFA for 2 h and then transferred to PBS at 4 °C. Fifty micrometer coronal sections of V1 were made using a Leica VT1000S vibratome (Leica Biosystems). Epitope retrieval was done by rinsing-free floating sections in PBS solution (pH 7.4). Sodium citrate buffer (10 mM, pH 8.5) was prepared and heated to 90 °C. Sections were placed in the buffer for 5 min and cooled down at room temperature. Sections were blocked by 5% goat serum, and β-catenin was stained by a monoclonal antibody (mouse-anti-β-catenin, 1:500, Transduction Laboratories), followed by goat-anti-mouse-Alexa488 (1:500; Invitrogen). PV was stained by a polyclonal antibody (rabbit-anti-parvalbumin 1:2000, Swant), followed by goat-anti-rabbit Alexa 568. β-Catenin expression was compared between β-catenin-deficient mice and their controls by measuring the mean signal of the image or in the area covering PV cell bodies. Sections were mounted on glass slides and embedded in Mowiol (10% (w/v) Mowiol 4-88, Calbiochem; 25% glycerol; 0.1 M Tris–HCl; pH 8.5) and stored at 4 °C.

Quantitative PCR

Total RNA (1.0 μg) was DNase I treated and used as a template to generate cDNA following the manufacturer's instructions (QuantiTect Reverse Transcription Kit-Qiagen) with a blend of oligo-dT and random hexamer primers. The reverse transcriptase reaction was incubated at 42 °C for 30 min and terminated at 95 °C for 3 min. The resulting cDNA was diluted 1:20 and served as a template in real-time qPCR assays (SYBR-Green PCR Master Mix; Applied Biosystems). Primers were generated for 4 Wnt target genes including Osteocalcin, Neurogenin1, SP5, and NeuroD1. Except Osteocalcin, all these transcripts were detected in mouse brain. These primers were tested for efficiency from which SP5 primer did not lead to satisfactory results. The determined transcript levels of these target genes were normalized against the levels of Gapdh and Hprt determined in the same sample to control for variability in the amount and quality of the RNA and the efficiency of the cDNA reaction. A more detailed explanation of the procedure has been explained elsewhere (Kamphuis et al. 2014).

Eyelid Suturing

Right eyelids were sutured under isoflurane anesthesia (www.abbott.com) by cutting the edge of every eyelid and joining the eyelids by a few sutures. A week later, the eyelids were opened right before the beginning of the measurements.

Single Unit Recordings

Single unit recordings were performed as previously described (Heimel et al. 2010). In short, mice were anesthetized by an intraperitoneal injection of urethane (200 mg/mL saline, 1.2 g/kg, Sigma) and subcutaneous injection of chlorprothixene (4 mg/mL distilled water, 8 mg/kg, Sigma). Recordings were made in the binocular part of V1, around 2.9 mm lateral and 0.5 anterior to the cranial landmark lambda. Contrast-tuning curves and some receptive-field sizes were measured with glass-coated tungsten 1 M micro-electrodes (Nano Bio Sensors). To find isolated units, the electrode was slowly forwarded until a spiking neuron was detected. Next, the electrode was advanced even more slowly to a position where the spike amplitudes of the neuron were well

above all other voltage fluctuations. If this was not possible, then the electrode would be advanced until another unit was found, or reinserted at a slightly different cortical location. This procedure gave very well-isolated units, but tended to over-represent the larger neurons in the deeper layers, which have relatively high spontaneous and evoked firing rates. Spikes were template matched by CED Spike2 and read by Matlab scripts for further analysis. Stimuli were projected to a 70 × 50 cm area on a large back-projection screen (Macada Innovision), positioned 50 cm away from the mouse. For receptive-field measurements using reverse correlation, a full-screen 7 × 5 grid of square black and white patches in a 34:1 ratio was presented for 5 min, randomly changing at 5 frames per second. The receptive-field size was taken as the approximate extent of all patches that were more than 3 standard deviations away from the mean intensity in the spike-triggered average. We determined contrast tuning with five 2-s-long presentations of full-screen square-wave gratings of 0.05 cycles per degree (cpd), drifting at 1 Hz in 1 of the 4 cardinal directions, shown at 20%, 40%, 60%, 75%, and 90% contrast. Recordings and analysis were done blind to genotype. Visual stimulation and analysis software for imaging and electrophysiology was written in Matlab (Mathworks) using the Psychophysics Toolbox (Brainard 1997). The code is available at https://github.org/heimel/InVivoTools.

Optical Imaging of Intrinsic Signal

Intrinsic optical signals were recorded from 4 to 6 months old β-catenin-deficient mice and their control littermates. The procedure has been described in detail previously (Heimel et al. 2007). Mice were anesthetized by an i.p. injection of urethane (Sigma-Aldrich, 200 mg/mL saline, 2 g/kg of body weight). To reduce mucus excretions, atropine sulfate (Teva Pharmachemie, 0.05 mg/mL saline, 0.1 mg/kg) was injected subcutaneously. In experiments related to contribution of NMDARs in measurement of cortical acuity, partial blockade of NMDARs was achieved by 15–30 mg/kg i.p. application of CGP 37849, which is a potent, selective, and competitive antagonist of NMDARs. This concentration is a number of times lower than 100 mg/kg suggested by previous studies (Pozza et al. 1990). The scalp was resected and images were acquired using an Optical Imager 3001 system (Optical Imaging) after illumination of the region of interest (ROI) by far red light (700 ± 30 nm). The stimulus monitor covered an area of the mouse visual field which ranged from −15° to 75° horizontally and −45° to 45° vertically. The retinotopic representation of V1 was mapped by drifting gratings that were shown in every quarter of the monitor. Full contrast, square-wave gratings of 0.05 cpd, moving at 2 Hz and changing direction every 0.6 s were shown every 15 s for 6 s in a pseudo-randomly chosen quadrant while the rest of the screen was a constant gray. For each pixel, the mean intensity during visual stimulation was computed, from which the intensity before stimulation was subtracted. Next, each pixel was assigned a color corresponding to the visual quadrant to which it had the least intensity, that is, the highest intrinsic signal response. For quantification of intrinsic signal responses of subsequent tests measuring ocular dominance (OD) and spatial frequency, we used this retinotopic map to manually define an ROI of pixels representing the upper nasal quadrant of the monitor in V1. An area outside V1, which was not responsive to visual stimuli, was determined as region of reference (ROR). The average signal in the ROI and ROR was computed as the change in intensity divided by the baseline intensity per pixel, across all the pixels in the specific regions. The response as the negative ratio of this signal in the ROI over the ROR signal was taken and was normalized to the stimulus onset and averaged from the first frame after stimulus onset until 2 s after stimulus offset. Measurements of spatial frequency tuning were made with 90% contrast sinusoidal reversing gratings that were presented in the top nasal quadrant for 3 s and changed directions every 0.75 s. Stimuli were randomly shown in 0.1, 0.2, 0.3, 0.4, 0.5, and 0.6 cpd and were followed by a 2 s, 50% gray contrast. The measurements were averages of 60 trials. Cortical acuity was determined by the zero-crossing of a least-squares fit with a threshold-linear function of the responses to the different spatial frequencies. This approach follows the preferred procedure for computing acuity from (human) sweep VEPs (Tyler et al. 1979). It takes the entire spatial frequency tuning curve into consideration, and it is insensitive to the absolute amplitude of the response at high spatial frequencies. In our previous work (Heimel et al. 2007), we have shown that in the spatial frequency range between 0.1 cpd and the mouse acuity limit, the intrinsic signal response is also well fitted by a linear function.

OD measurements were performed by showing visual stimuli in the upper nasal quadrant of the screen alternatively to contralateral and ipsilateral eyes. These stimuli were shown once every 17 s for 3 s, while the shutter remained open for 6 s during which imaging was performed. The Ocular Dominance Index (ODI) was calculated as (contralateral response − ipsilateral response)/(contralateral response + ipsilateral response). Visual stimuli consisted of square wave gratings with 90% contrast, 0.05 cpd, and temporal frequency of 2 Hz, which changed directions every 0.6 s and lasted 3 s. The same procedure was repeated when both eye shutters were closed to make sure that vision was blocked in both eyes. The ODI value for each mouse was the mean of 40 trial measurements.

Statistical Analysis and Contrast-Tuning Curve Fitting

Two-tailed unpaired Student's *t*-tests were used for all comparisons in which the data passed Shapiro–Wilk normality test. Western blotting data, immunohistochemistry, AMPA/NMDA ratio, inter-event interval, and amplitude averages of mEPSCs in β-catenin-deficient mice versus their controls were compared for statistical significance by a Mann–Whitney test. Comparisons between paired groups were done by Wilcoxon signed-rank test. Firing rates of neurons in response to steps of current injections were compared by one-way ANOVA. ODIs were compared between β-catenin-deficient mice and their controls littermates by two-way ANOVA, followed by Tukey's test for correction of multiple comparisons. Contrast-tuning curves were fit with a Naka–Rushton curve by minimizing the least squared error using a Nelder–Mead procedure in Matlab. A null-response point at 1% contrast was added to constrain the fit. Minimization was initiated with semisaturation constant $\sigma = 0.4$ and exponent $n = 2$. C50, the contrast at which the response is half its maximum, was determined from the fit.

Results

Inactivating the β-Catenin Gene in Excitatory Neurons of the Adult Cortex

In order to inactivate β-catenin in excitatory cortical neurons of adult mice, we crossed mice carrying a floxed β-catenin locus (Junghans et al. 2005) to G35-3 cre transgenic mice (Sawtell et al. 2003; Dahlhaus et al. 2008) in which efficient cre-recombinase expression starts after 4–5 weeks of age and is restricted to excitatory neurons of the hippocampus and cortex (Sawtell et al.

2003; Dahlhaus et al. 2008). Using immunohistochemistry, we analyzed the expression of β-catenin in V1 of mice in which the gene encoding β-catenin was inactivated in cortical excitatory neurons (referred to as β-catenin-deficient mice) and control littermates (Fig. 1A–D). In littermate controls, it was clear that β-catenin is predominantly expressed on the cell surface and neuropil and excluded from the cytoplasm and nuclei of cortical neurons (Fig. 1A,D). Such a differential expression has also been reported in hippocampus (Mills et al. 2014) and supports the finding of our quantitative PCR experiments that transcription of Wnt target genes is not changed in β-catenin-deficient mice (Supplementary Fig. 1). In β-catenin-deficient mice, expression of the protein in V1 was strongly reduced compared with control littermates (control mice 47.9 ± 2.9, $n = 33$ sections from 3 mice vs. β-catenin-deficient mice 25.7 ± 2.5, $n = 22$ sections from 3 mice, $P < 0.001$) (Fig. 1B). Some expression remained, possibly due to β-catenin expression in glia, interneurons or projections from non-cortical brain areas such as the thalamus. Parvalbumin (PV) expressing neurons did not show a similar decrease in β-catenin signal in β-catenin-deficient mice (control mice 18.5 ± 1, 34 neurons, 3 mice vs. β-catenin-deficient mice 15 ± 1.8, 21 neurons, 3 mice, $P = 0.07$) (Fig. 1C).

Changes in β-Catenin Interacting Proteins in Synaptic Membranes of β-Catenin-Deficient Mice

β-Catenin has been identified as a critical factor in linking N-cadherin to the actin cytoskeleton through dynamic interaction with α-catenin (Drees et al. 2005; Yamada et al. 2005). Moreover, it was found that the activity-regulated interaction of β-catenin with N-cadherin increases the localization of N-cadherin at the synapse by reducing its endocytosis (Tai et al. 2007). We therefore analyzed whether the levels of β-catenin, N-cadherin, and α-catenin were altered in synaptic membranes prepared from β-catenin-deficient animals. Western blot analyses showed that as expected, β-catenin (100 ± 13%, $n = 3$ mice vs. 27 ± 17%, $n = 5$ mice; $P < 0.05$) and α-catenin (100 ± 10% vs. 39 ± 16%; $P < 0.05$) levels were reduced (Fig. 1E). N-cadherin levels appeared lower but the decrease was not significant (100 ± 23% vs. 65 ± 19%; $P = 0.19$). Actin levels remained unchanged (100 ± 14% vs. 117 ± 12%; $P = 0.46$). γ-Catenin has a high homology to β-catenin and interacts with N-cadherin and α-catenin. As γ-catenin was previously found to partially compensate for the loss of β-catenin in hepatocytes (Wickline et al. 2011), we tested whether this was also the case in the cortex of β-catenin-deficient mice. Indeed, we detected a strong increase in γ-catenin levels in synaptic membranes of β-catenin deficient V1 (100 ± 21% vs. 354 ± 10%; $P < 0.05$) (Fig. 1E). Thus, the lack of β-catenin caused down-regulation of α-catenin while γ-catenin was strongly upregulated, possibly compensating for the loss of β-catenin.

Cortical Acuity is Reduced in β-Catenin-Deficient Mice

We first assessed whether the absence of β-catenin in excitatory neurons of adult V1 had any effects on visually evoked cortical responses. Visual responses to high-contrast phase-reversing sinusoidal gratings of different spatial frequencies were measured using optical imaging of intrinsic signal and cortical acuity (defined as the null-response point of a threshold-linear curve fitted to the data) was determined in anesthetized β-catenin-deficient mice and their control littermates (Fig. 2A–D). We found that while responses to low spatial frequency stimuli were unaffected, high spatial frequency stimuli elicited strongly decreased responses in β-catenin-deficient mice (control mice 0.45 ± 0.04 cpd, $n = 8$ vs. β-catenin-deficient mice 0.29 ± 0.03, $n = 9$, $P < 0.01$), thus revealing a decrease in cortical acuity (Fig. 2D,E).

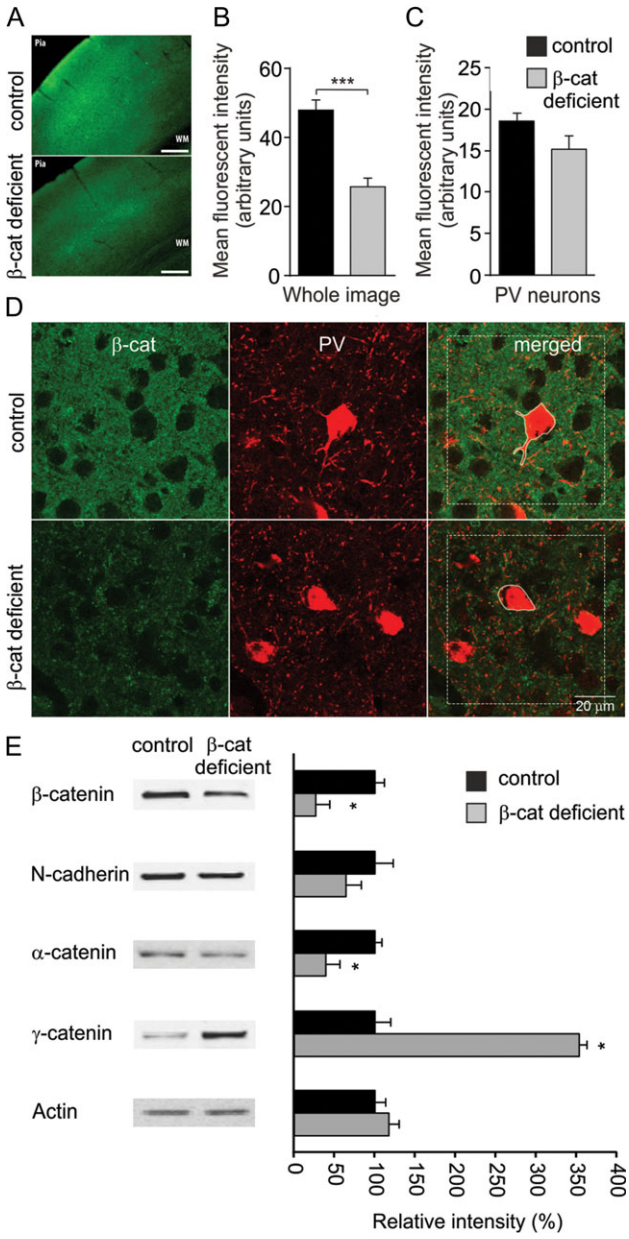

Figure 1. Ablation of β-catenin in excitatory neurons changes expression levels of other catenins. (*A*) Immunohistochemical staining for β-catenin in V1 after epitope retrieval showed a decreased intensity in β-catenin-deficient mice. Scale bar 200 μm. (*B*) Quantification of average fluorescence intensity in V1. (*C*) Quantification of average fluorescence intensity on PV cells. β-Catenin signal is significantly reduced in β-catenin KO mice compared with the controls while the same signal in PV cell bodies does not undergo a similar decrease. (*D*) Examples of co-staining for β-catenin and PV in V1 of β-catenin deficient and control mice. β-Catenin expression was measured as average intensity of green signal in the dashed white square area, which contains many neurons, and specifically in PV neurons delineated by solid white line. (*E*) Western blotting of synaptic membranes extracted from V1 of β-catenin mice and control littermates showed a significant reduction in β-catenin and α-catenin expression and a strong increase in γ-catenin expression in β-catenin-deficient mice relative to controls. There was no significant change in N-cadherin expression. Representative blots of the above-mentioned proteins as well as actin as a loading control are shown in the left panel. WM represents white matter. Error bars denote standard error of mean (SEM) (*$P < 0.05$, ***$P < 0.01$, Mann–Whitney).

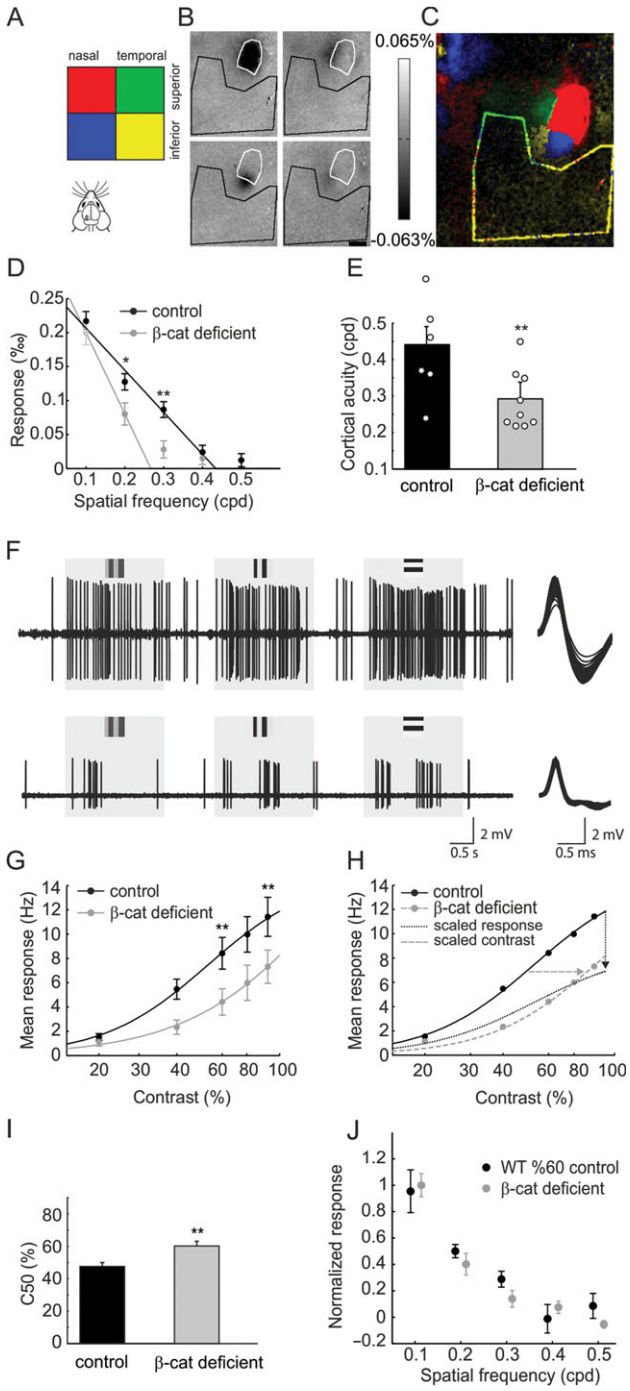

Figure 2. Contrast sensitivity and cortical acuity are reduced in V1 of β-catenin-deficient mice. (*A*) Schematic of experimental setup for retinotopy and measurement of cortical acuity and OD index. (*B*) Raw images of responses to drifting gratings shown in the different quadrants of the stimulus monitor to determine retinotopy and (*C*) their pseudo-colored combination. ROI and ROR are drawn in white and black, around responsive areas and the rest of the cortex, respectively. (*D*) Decreased visual responses to high-contrast phase-reversing sinusoidal gratings of high spatial frequencies in β-catenin-deficient mice compared with controls measured by optical imaging of intrinsic signal. (*E*) Decreased cortical acuity of β-catenin-deficient mice compared with their littermate controls. (*F*) Examples of two single unit recordings (left) and their spike forms (right). Gray boxes represent the time that visual stimuli were presented. Small squares close to the upper side of the gray boxes represent the orientation and contrast of the stimuli that were used. All spikes in the traces are smoothed and then superimposed. (*G*) Average population responses were lower in β-catenin-deficient mice. The data are fitted with Naka–Rushton curves. (*H*) Best fit of data from control mice to the responses of β-catenin-deficient mice was achieved by reducing contrast (gray dashed line), and not by reducing response strength (black dotted line). (*I*) Single unit recordings showed that C50, the contrast at which half the maximum response is elicited, was higher in β-catenin-deficient mice than in controls. (*J*) At different spatial frequencies, responses of V1 neurons in β-catenin-deficient mice to 90% contrast stimuli match the responses of control mice to the same stimuli at 60% contrast. Error bars denote SEM (**$P < 0.01$).

Reduced Contrast Sensitivity Causes a Deficit in Spatial Frequency Tuning in β-Catenin-Deficient Mice

Reduced cortical acuity can be caused via three different functional mechanisms (Heimel et al. 2010). The first mechanism is enlargement of receptive fields of neurons in the visual cortex. Our measurement of receptive field sizes, performed by single unit recordings (Fig. 2*F*), revealed that they were unaffected in β-catenin-deficient mice (control 19.4 ± 0.7°, $n = 90$ cells from 10 mice vs. β-catenin-deficient mice 18.5 ± 0.7°, $n = 76$ cells from 10 mice, $P = 0.37$) (Supplementary Fig. 2A).

The second mechanism through which cortical acuity could diminish is a decrease in signal to noise ratio. Because responses to high spatial frequency stimuli are weaker, they are relatively more affected by noise. Therefore, we measured signal to noise ratio in two different ways. The first approach involved recording single unit activity with or without visual stimuli, representing signal and noise activity levels, respectively. This revealed no differences between β-catenin-deficient mice and control littermates (spontaneous rate: control 4.9 ± 0.6 Hz, $n = 118$ cells vs. β-catenin deficient 4.6 ± 0.6 Hz, $n = 114$ cells, $P = 0.75$, Supplementary Fig. 2B; evoked peak rate: control 11.3 ± 1 Hz, $n = 90$ cells from 10 mice vs. β-catenin deficient 9.4 ± 0.9 Hz, $n = 76$ cells from 10 mice, $P = 0.17$) (Supplementary Fig. 2C). In the second approach, we measured the responses of single neurons when the stimuli were presented inside or outside their receptive fields. The results are presented as the area under receiver operating characteristic curve that defines the detectability of a stimulus at the center of the receptor field. This approach also showed that signal to noise ratios were unaffected by the β-catenin mutation (control 0.90 ± 0.02, $n = 90$ cells from 10 mice vs. β-catenin deficient 0.89 ± 0.02, $n = 76$ cells from 10 mice) (Supplementary Fig. 2D).

The third mechanism is a reduction in perceived contrast (Heimel et al. 2010). We therefore assessed whether loss of β-catenin in adulthood affected the responses of individual neurons to visual stimuli of varying contrasts. Single unit recordings showed that stimuli with higher contrast had to be presented to β-catenin-deficient mice in order to elicit responses of the same strength as observed in control animals (Fig. 2*G*,*H*). Scaling the contrast-axis resulted in a better fit of the contrast response curve of the β-catenin-deficient mice with that of the control animals than scaling the response-axis (Fig. 2*G*, optimal contrast scale factor was 1.72, mean squared error in fit 0.31; Fig. 2*H*, optimal response scale factor was 0.58, mean squared error in fit was 1.5), showing there is a reduction in contrast sensitivity rather than a general reduction in cortical responsiveness. This is also apparent in the increase of C50, the contrast at which half the maximum response is reached, from 48% in controls, $n = 72$ cells from 9 mice, to 60%, $n = 44$ cells from 8 mice, in β-catenin-deficient animals ($P < 0.01$, Fig. 2*I*). The decrease in perceived contrast is so that the responses of β-catenin-deficient mice to 90% contrast stimuli are the same as those of control mice to 60% contrast stimuli (Fig. 2*J*). As we showed previously, reduced

contrast sensitivity affects responses to high spatial frequency more than those to low spatial frequency due to cortical gain control (Heimel et al. 2010). This is because strong responses to low spatial frequencies are strongly normalized, causing them to change little at lower contrast. Weak responses to high spatial frequencies are barely normalized, however, and reduce considerably when contrast is lowered. We conclude that the loss in contrast sensitivity was responsible for the decrease in spatial frequency tuning response in β-catenin-deficient mice.

Presynaptic Function Appears Unaltered in the Absence of β-Catenin

We have previously shown that reduced synaptic efficacy can reduce contrast sensitivity and cortical acuity (Heimel et al. 2010). We therefore asked whether synaptic function was altered by the β-catenin deficiency. It was previously reported that in hippocampal slices of β-catenin-deficient mice the number of reserve pool synaptic vesicles was reduced, causing increased synaptic depression during high-frequency stimuli (Bamji et al. 2003). We therefore tested whether there was a presynaptic deficit in the visual cortex of adult β-catenin-deficient mice. We used local field potential recordings to assess the level of synaptic depression induced in layers 2/3 and 4 of V1 slices by continuous high-frequency stimulation (80 stimuli at 14 Hz) of white matter. We found that synaptic depressions in β-catenin-deficient mice and control littermates were indistinguishable, both in layers 2/3 (54.2 ± 1.7%, $n = 9$ mice vs. 55.7 ± 3.6%, $n = 7$ mice $P = 0.70$) and layer 4 (64.9 ± 3.6%, $n = 10$ vs. 64 ± 5.0%, $n = 7$, $P = 0.95$) (Fig. 3A). Moreover, no changes in paired-pulse facilitation were observed (1.15 ± 0.07, $n = 10$ mice vs. 1.11 ± 0.05, $n = 7$ mice, $P = 0.70$ for layer 2/3 and 1.03 ± 0.04, $n = 10$ mice vs. 1.13 ± 0.05, $n = 7$ mice, $P = 0.11$ for layer 4) (Fig. 3B). We conclude that β-catenin deficiency in adult mice does not cause significant presynaptic deficits in excitatory neurons of adult V1.

Inactivation of β-Catenin Does Not Affect Intrinsic Excitability

Experiments in cultured cortical slices also revealed that intrinsic excitability was reduced due to changes in the organization of the axon initial segment when β-catenin expression was knocked-down using shRNA (Tapia et al. 2013). However, current clamp recordings from layers 2/3 of V1 pyramidal neurons did not reveal any changes in intrinsic excitability in adult visual cortical slices of β-catenin-deficient mice ($n = 19$ from 7 mice), compared with their control littermates ($n = 8$ slices from 4 mice, one-way ANOVA, $F_{1,25} = 0.72$, $P = 0.4$) (Fig. 3C).

NMDAR Function is Diminished in β-Catenin-Deficient Mice

We next analyzed whether the inactivation of β-catenin in adult V1 caused postsynaptic deficits. In hippocampal dissociated cell cultures, it was previously observed that β-catenin deficiency results in changes in AMPAR-mediated synaptic transmission as illustrated by reduced mEPSC amplitudes (Okuda et al. 2007). Increased synaptic localization of β-catenin due to reduced phosphorylation at tyrosine 654 increased mEPSC frequencies (Murase et al. 2002). In contrast, β-catenin overexpression during very early development, both in vivo and in vitro, can result in a reduction of mEPSC amplitudes without affecting frequencies (Peng et al. 2009).

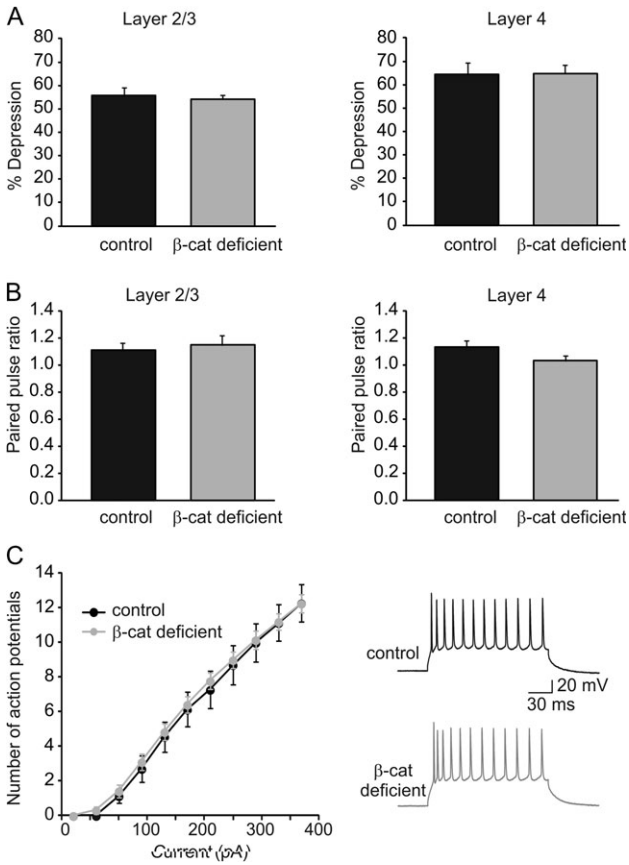

Figure 3. Ablation of β-catenin in excitatory neurons does not cause a presynaptic deficit or changes in action potential generation. (A) Synaptic depression induced in layers 2/3 and 4 of V1 slices by continuous stimulation (80 stimuli at 14 Hz) of white matter was not different in β-catenin-deficient mice compared with their control littermates. Averages of responses to the last 5 stimuli are normalized to the average of responses to the first 5 stimuli. (B) Paired-pulse ratios measured in both layer 2/3 and 4 by 40 Hz stimulations of white matter were also unchanged in β-catenin-deficient mice. (C) Number of action potentials in response to depolarizing current steps in layer 2/3 pyramidal neurons of β-catenin-deficient mice was indistinguishable from those of their control littermates. Right panel: example traces of action potentials of pyramidal neurons in response to a depolarizing current injection. Error bars denote SEM.

To test whether AMPAR-mediated synaptic transmission was affected, we performed whole-cell patch clamp recordings to record mEPSCs in layer 2/3 pyramidal neurons in V1 slices of β-catenin-deficient animals and control littermates. We found that mEPSC amplitudes were unchanged (15.3 ± 0.3 pA, $n = 28$ cells from 12 mice vs. 15.6 ± 0.3 pA, $n = 16$ cells from 9 mice, $P = 0.30$) (Fig. 4A). mEPSC interval times in β-catenin-deficient mice were not statistically different (218 ± 17 ms, $n = 28$ cells from 12 mice vs. 173 ± 18 ms, $n = 16$ cells from 9 mice, $P = 0.09$) (Fig. 4B).

We also analyzed whether the NMDAR contribution to excitatory synaptic transmission was reduced. To this end, we recorded NMDA/AMPA ratios in L2/3 pyramidal neurons in V1. EPSCs were evoked by extracellular stimulation nearly 100 μm lateral to the recorded neuron while the neuron was held either at −80 mV to determine the AMPAR contribution, or at +40 mV to determine the NMDAR contribution. We found that NMDA/AMPA ratios were significantly decreased in β-catenin-deficient mice (Fig. 4C, control: 0.32 ± 0.02, $n = 22$ cells from 5 mice vs. β-catenin-deficient mice: 0.246 ± 0.017, $n = 21$ from 9 mice, $P < 0.01$). Since mEPSC amplitude did not change, suggesting

that postsynaptic AMPAR properties were unaltered, this decrease in NMDA/AMPA ratio most likely reflects a reduction in synaptic NMDAR currents.

NMDARs can be recruited to synapses through interacting with the scaffolding protein S-SCAM, which binds to the PDZ-binding domain of β-catenin (Nishimura et al. 2002; Danielson et al. 2012). It is thus possible that in the absence of β-catenin, S-SCAM-mediated recruitment of NMDARs is affected. To test this, we performed western blot experiments and assessed whether S-SCAM or NMDAR levels were reduced in synaptic membrane fractions of β-catenin-deficient mice. We found that S-SCAM expression was significantly reduced (control mice 100 ± 8%, $n = 5$ mice vs. β-catenin-deficient mice 66 ± 11%, $n = 7$ mice; $P < 0.05$) (Fig. 4D). As could be expected, NMDAR 2A/B levels were also significantly reduced in synaptic membranes isolated from V1 of β-catenin-deficient mice (100 ± 6% vs. 68 ± 11%; $P < 0.05$) (Fig. 4D). We conclude that β-catenin deficiency in adult V1 causes a reduction in postsynaptic NMDAR-mediated currents, while other aspects of synaptic transmission are surprisingly intact.

Reducing NMDAR Current Decreases Cortical Acuity

NMDARs are known to play a role in synaptic transmission and have been reported to be directly involved in responses of V1 to visual stimuli (Tsumoto et al. 1987; Fox et al. 1989, 1990; Miller et al. 1989; Self et al. 2012). To confirm that decreased NMDAR current can directly affect spatial frequency tuning response, we performed measurements in wildtype mice before and after partial blockade of NMDARs by i.p. injection of CGP 37849 (15–30 mg/kg), a selective and competitive antagonist of NMDARs (Fig. 5A). We noticed a significant decrease in spatial frequency tuning responses after injection of CGP 37849 (0.53 ± 0.05 cpd vs. 0.37 ± 0.04 cpd, $n = 8$ mice, before and after injection of the blocker, Wilcoxon signed-rank, $P < 0.01$, Fig. 5B), while application of saline did not affect cortical acuity (0.57 ± 0.04 cpd vs. 0.62 ± 0.06 cpd, $n = 6$ mice, before and after injection of saline, Wilcoxon signed-rank, $P = 0.10$, Fig. 5C). Overall, these results support the possibility that diminished NMDAR current is the underlying cause of decreased cortical acuity in β-catenin-deficient mice.

Unchanged OD Plasticity in the Absence of Cortical β-Catenin

Previous work has shown that deletion of NMDARs in excitatory neurons in V1 interferes with adult OD plasticity (Sawtell et al. 2003). Therefore, we addressed whether the observed change in the NMDA/AMPA ratio in V1 of adult β-catenin-deficient mice also affects OD plasticity. We used optical imaging of intrinsic signal to determine the amount of OD plasticity induced by 1 week of monocular deprivation (Fig. 5D). The ODI shifted to a similar degree in control mice and β-catenin-deficient littermates (from 0.49 ± 0.04 in undeprived control mice, $n = 8$ to 0.24 ± 0.05 in deprived control mice $n = 7$, $P < 0.05$, and from 0.41 ± 0.05 in undeprived β-catenin-deficient mice, $n = 8$ to 0.18 ± 0.09 in deprived β-catenin-deficient mice, $n = 5$, $P < 0.05$, two-way ANOVA, $F(1, 24) = 19.57$ ($P < 001$) followed by Tukey's test). The ODI values of β-catenin-deficient mice or control littermates were not different in undeprived ($P = 0.68$) or deprived ($P = 0.92$) mice, two-way ANOVA, $F(1, 24) = 1.47$ ($P = 0.24$). We conclude that β-catenin is not essential for this form of adult cortical plasticity.

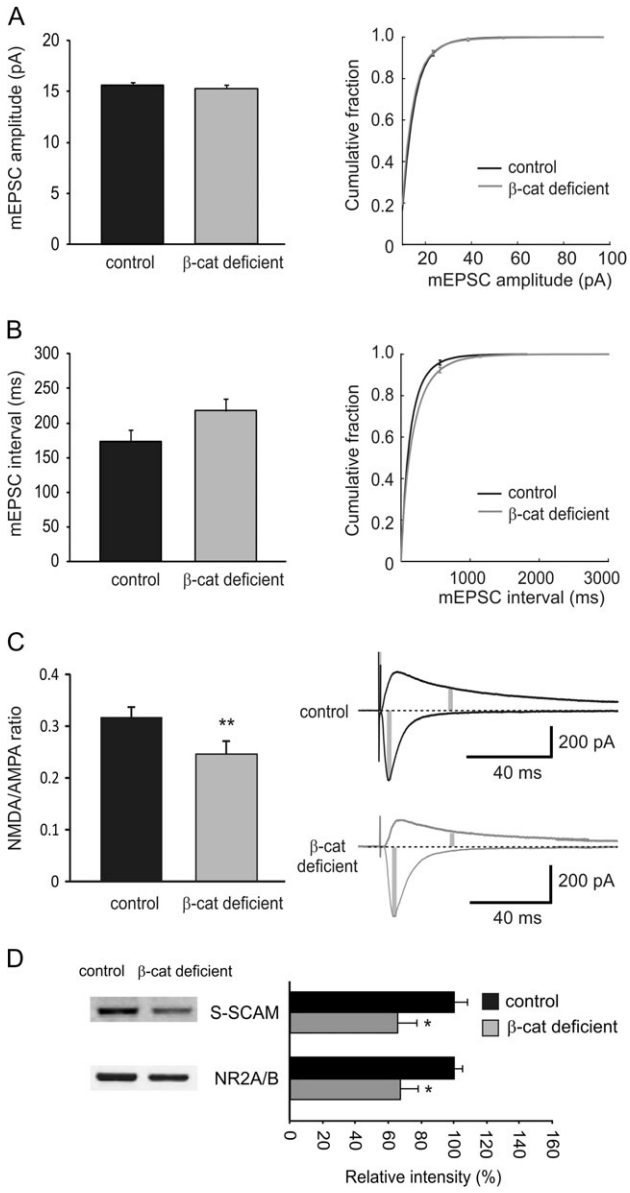

Figure 4. Unaltered mEPSCs but attenuated NMDA currents in β-catenin-deficient mice. Loss of β-catenin did not cause significant changes in (*A*) mEPSC amplitudes or (*B*) intervals of layer 2/3 pyramidal neurons in V1. (*C*) Ratio of NMDA to AMPA current was significantly decreased in layer 2/3 of β-catenin-deficient V1 compared with control littermates. Right: example traces of AMPA receptor-mediated EPSCs (downward currents; recorded at −80 mV) and NMDA-receptor-mediated EPSCs (upward currents; recorded at +40 mV). Gray bars indicate time-points used for AMPA and NMDA current measurement. (*D*) Western blotting of synaptic membranes extracted from V1 showed a significant reduction in S-SCAM and NR2A/B levels in β-catenin-deficient mice ($n = 7$) relative to controls ($n = 5$). Representative blots of the above-mentioned proteins are shown in the left panel. Error bars denote SEM (*$P < 0.05$, **$P < 0.01$).

Discussion

Here we show that β-catenin in excitatory neurons of the adult neocortex is essential for the optimal processing of visual information. Underlying the visual deficit observed in β-catenin-deficient mice appears to be a decrease in synaptic NMDAR levels, while other pre- and postsynaptic properties of excitatory neurons are unaltered in the absence of β-catenin.

Interestingly, our findings in adult V1 differ from what has been observed when β-catenin is inactivated during development or in neuronal cultures (Tang et al. 1998; Goda 2002; Murase et al. 2002; Bamji et al. 2003; Schuman and Murase 2003; Okuda et al. 2007; Tai et al. 2007; Vitureira et al. 2012). These studies showed that the cadherin–β-catenin adhesion complex is involved in the regulation of postsynaptic AMPARs levels. This is illustrated by the observation that in dissociated hippocampal cultures, deletion of β-catenin causes dendritic spines to become thinner and amplitudes of mEPSC to become smaller (Okuda et al. 2007). Both β-catenin's cadherin-binding domain and its C-terminal PDZ-binding domain, which allows β-catenin to associate with synaptic scaffold proteins, are essential for this role of β-catenin (Okuda et al. 2007). The interactions between β-catenin and N-cadherin can also directly (Bamji et al. 2003; Sun et al. 2009) or indirectly (Murase et al. 2002) affect presynaptic vesicle release resulting in increased synaptic depression or decreased mEPSC frequencies, respectively.

Our experiments show that in adult V1, inactivating the β-catenin gene in excitatory neurons does not significantly affect the frequency or amplitude of mEPSCs. We also find no evidence for increased synaptic depression upon prolonged high-frequency stimulation. One explanation for this apparent discrepancy could be that β-catenin carries out different functions throughout neuronal development. The cadherin–β-catenin complex may be more important for regulating presynaptic efficacy at developmental stages when the dynamics of neurite growth and -retraction and synapse turnover are still high. This is supported by a study showing that inactivation of N-cadherin in the adult hippocampus does not affect spine morphology or basic synaptic transmission, while it does in neuronal cultures or during development (Bozdagi et al. 2010). Alternatively, compensatory mechanisms for a deficiency in N-cadherin or β-catenin, such as the upregulation of its homolog γ-catenin, which we observed, may become more effective in the adult cortex.

An additional explanation for the differences between our findings and previous work may lie in the low percentage of genetically targeted neurons in neuronal cultures compared with the broad genetic targeting in the β-catenin-deficient mice we studied. Several recent studies have shown that interfering with neuroligin expression or BDNF/TrkB signaling in isolated cortical neurons causes changes in neuronal function and morphology that do not occur when all neurons are targeted (Kwon et al. 2012; Saiepour et al. 2015). This suggests that synaptic competition may enhance the consequences of synaptic malfunction. In line with this idea is the recent finding that activity-dependent synaptic plasticity and -stability were

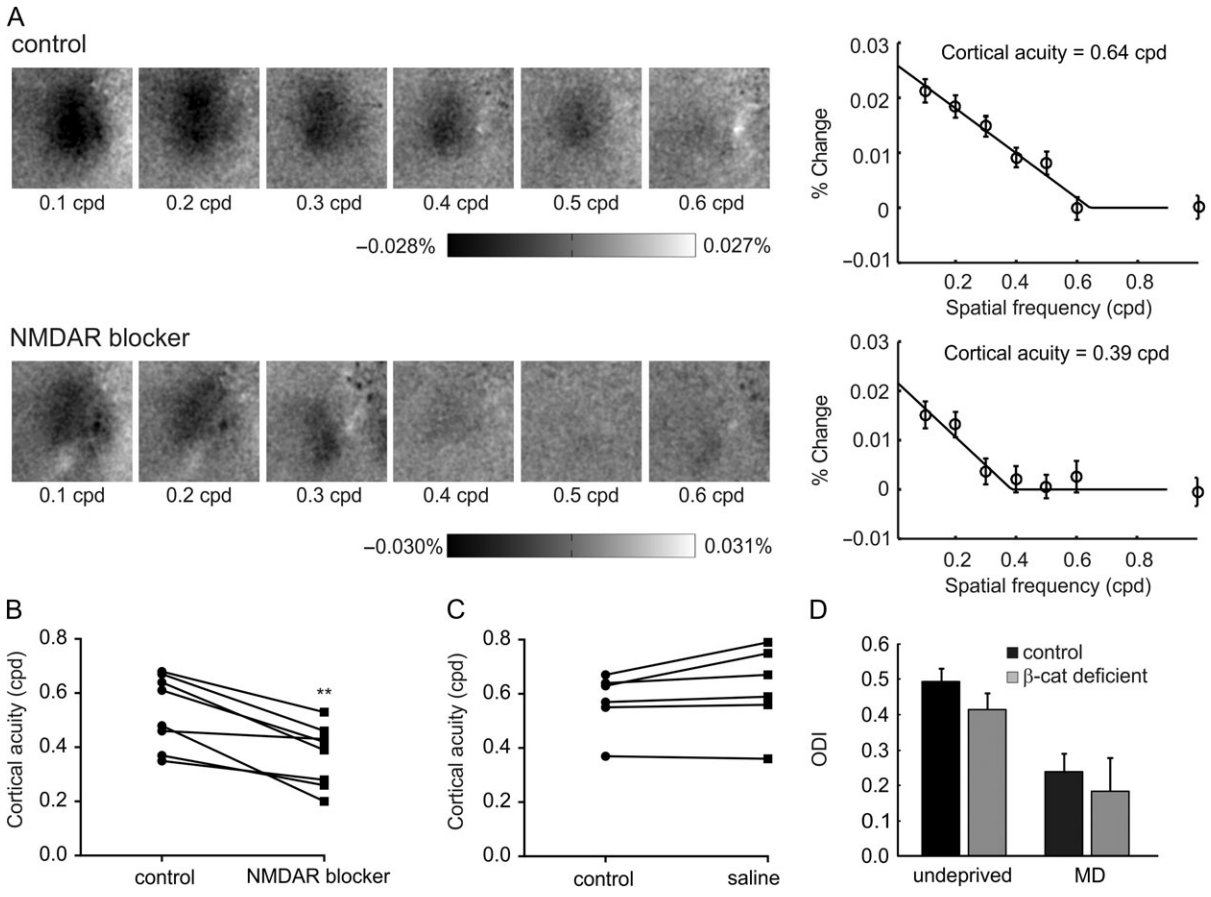

Figure 5. Cortical acuity is diminished after partial blockade of NMDA receptors. (*A*) Raw responses of the binocular V1 to sinusoidal gratings of increasing spatial frequencies, without (upper row) or with NMDA blocker (lower row). Application of CGP 37849 deceases the responses to sinusoidal gratings stimuli (lower row). Rectangles with black to white gradients indicate the maximum change in response for pixels of the upper rows. Cortical acuity was determined by the zero-crossing of a least-squares fit with a threshold-linear function (right panels). (*B*) Partial blockade of NMDA receptors by intraperitoneal application of CGP 37849 decreases cortical acuity. (*C*) Injection of saline has no significant effect on cortical acuity. (*D*) Ocular dominance plasticity, induced by 7 days of monocular deprivation in adult β-catenin-deficient mice (nondeprived, $n = 8$, deprived, $n = 5$) is not different from that of control littermates (nondeprived, $n = 8$, deprived, $n = 7$, two-way ANOVA). Error bars denote SEM (*$P < 0.05$, **$P < 0.01$).

changed after genetically targeting GSK3β or expression of a stabilized form of β-catenin in individual neurons of the adult cortex (Ochs et al. 2015). Another recent study provides evidence for both explanations (Bian et al. 2015). This study found that inactivating β-catenin in all cortical neurons selectively reduced the pruning of thin spines during development. However, deleting β-catenin in individual neurons also caused loss of mature spines through a competitive mechanism.

While we find that AMPAR-mediated synaptic transmission appears unaltered, NMDAR levels are diminished upon deletion of β-catenin. Whole-cell patch clamp recordings in layer 2/3 pyramidal neurons showed that NMDA/AMPA ratios are significantly reduced in these mice. NMDARs interact with the synaptic scaffolding protein S-SCAM, which associates with the PDZ-binding domain of β-catenin. This interaction has previously been implicated in the maintenance of synaptic NMDARs (Nishimura et al. 2002). Since S-SCAM levels are reduced in synaptic membranes from β-catenin-deficient V1, this maintenance of synaptic NMDARs could be disturbed. Interestingly, S-SCAM is also known to interact with neuroligin-1, and neuroligin-1 deficiency can also cause a reduction in NMDA/AMPA ratios (Kwon et al. 2012). Therefore, this pathway may provide an alternative explanation of the observed changes in NMDAR levels in β-catenin-deficient V1.

NMDARs play an important role in synaptic plasticity in the cortex (Artola and Singer 1987; Kleinschmidt et al. 1987). They are critical for OD plasticity in the juvenile as well as in adult V1 (Sawtell et al. 2003; Sato and Stryker 2008). However, the observed reduction in NMDAR function in adult β-catenin-deficient mice did not affect adult OD plasticity possibly due to the modest decrease in synaptic NMDAR levels. It was previously found that β-catenin is essential for plasticity in the adult amygdala (Maguschak and Ressler 2008). More recently, it was found that β-catenin overexpression interfered with hippocampal learning and long-term depression (Mills et al. 2014). Our findings thus suggest that plasticity in amygdala and hippocampus recruit different plasticity mechanisms than OD plasticity in V1, as previously noted (Hensch et al. 1998).

Previous studies in which NMDAR function was blocked pharmacologically using APV have shown that NMDARs also contribute strongly to visual responses in V1 (Tsumoto et al. 1986, 1987; Fox et al. 1989, 1990; Miller et al. 1989; Tsumoto 1990; Self et al. 2012). In line with these earlier observations, we found that the reduced functionality of NMDARs in β-catenin-deficient mice is associated with reduced responsiveness of neurons in V1 to specific visual stimuli. In order for V1 of β-catenin-deficient mice to show responses similar to those in control littermates, the contrast of the stimuli had to be significantly increased. This reduction in contrast sensitivity in β-catenin-deficient mice is highly reminiscent of what we have previously observed in transgenic mice expressing the dominant negative BDNF-receptor TrkB.T1 in pyramidal neurons of the adult neocortex (Heimel et al. 2010). In these mice, the reduced contrast sensitivity caused a decrease in cortical acuity, similar to what we observe in β-catenin-deficient mice. As receptive fields and signal to noise levels of V1 neurons in β-catenin-deficient mice were unchanged, we conclude that the spatial frequency tuning response phenotype in β-catenin-deficient mice is due solely to a decrease in contrast sensitivity. This confirms the previously described effect of contrast reduction on high-resolution vision and shows that different synaptic deficits can cause a highly similar visual deficit.

Our findings in β-catenin-deficient mice have some interesting parallels with observations made in ASD patients. For example, problems in low level processing of visual inputs (Pei et al. 2014) and deficits in responses to low-contrast stimuli have also been observed in children with ASD (Weinger et al. 2014). Moreover, ASD is associated with NMDAR dysfunction (Lee et al. 2015). The dominant effect of β-catenin levels on NMDAR currents in the adult cortex may thus provide an interesting link between mutations in the β-catenin gene and the pathogenesis of ASD. NMDAR dysfunction has also been implicated in schizophrenia. As clozapine, haloperidol, and risperidone have been shown to increase β-catenin levels, there may also be a link between the action of these antipsychotics, β-catenin expression, and the regulation of NMDAR currents. Novel insights in the contribution of β-catenin in adult synaptic function may thus help to better understand the pathogenesis of neurodevelopmental disorders and their treatment.

Supplementary Material

Supplementary material are available at *Cerebral Cortex* online.

Funding

AgentschapNL to the Neuro-Basic PharmaPhenomics consortium, a Vidi grant from NWO to C.N.L., NWO-ALW grant 823.02.001, a gift from Praktijkgenerator b.v. and a Veni grant from NWO to R.M. (NWO 863.12.006).

Notes

The authors would like to thank Dr Helmut Kessels for the critical reading of the manuscript and Emma Ruimschotel for technical assistance and Drs Geeske van Woerden, Ype Elgersma, and Ka Wan Li for help with protein- and gene expression experiments. *Conflict of Interest*: None declared.

References

Abe K, Takeichi M. 2007. NMDA-receptor activation induces calpain-mediated beta-catenin cleavages for triggering gene expression. Neuron. 53:387–397.

Alimohamad H, Rajakumar N, Seah YH, Rushlow W. 2005. Antipsychotics alter the protein expression levels of beta-catenin and GSK-3 in the rat medial prefrontal cortex and striatum. Biol Psychiatry. 57:533–542.

Artola A, Singer W. 1987. Long-term potentiation and NMDA receptors in rat visual cortex. Nature. 330:649–652.

Bamji SX, Shimazu K, Kimes N, Huelsken J, Birchmeier W, Lu B, Reichardt LF. 2003. Role of beta-catenin in synaptic vesicle localization and presynaptic assembly. Neuron. 40:719–731.

Barker N, Morin PJ, Clevers H. 2000. The Yin-Yang of TCF/beta-catenin signaling. Adv Cancer Res. 77:1–24.

Beaulieu JM, Gainetdinov RR, Caron MG. 2009. Akt/GSK3 signaling in the action of psychotropic drugs. Annu Rev Pharmacol Toxicol. 49:327–347.

Bian WJ, Miao WY, He SJ, Qiu Z, Yu X. 2015. Coordinated spine pruning and maturation mediated by inter-spine competition for cadherin/catenin complexes. Cell. 162:808–822.

Bozdagi O, Shan W, Tanaka H, Benson DL, Huntley GW. 2000. Increasing numbers of synaptic puncta during late-phase LTP: N-cadherin is synthesized, recruited to synaptic sites, and required for potentiation. Neuron. 28:245–259.

Bozdagi O, Valcin M, Poskanzer K, Tanaka H, Benson DL. 2004. Temporally distinct demands for classic cadherins in synapse formation and maturation. Mol Cell Neurosci. 27:509–521.

Bozdagi O, Wang XB, Nikitczuk JS, Anderson TR, Bloss EB, Radice GL, Zhou Q, Benson DL, Huntley GW. 2010. Persistence of coordinated long-term potentiation and dendritic spine enlargement at mature hippocampal CA1 synapses requires N-cadherin. J Neurosci. 30:9984–9989.

Brainard DH. 1997. The psychophysics toolbox. Spat Vis. 10: 433–436.

Brigidi GS, Bamji SX. 2011. Cadherin-catenin adhesion complexes at the synapse. Curr Opin Neurobiol. 21:208–214.

Bureau I, von Saint PF, Svoboda K. 2006. Interdigitated paralemniscal and lemniscal pathways in the mouse barrel cortex. PLoS Biol. 4:e382.

Chakravarthy S, Saiepour MH, Bence M, Perry S, Hartman R, Couey JJ, Mansvelder HD, Levelt CN. 2006. Postsynaptic TrkB signaling has distinct roles in spine maintenance in adult visual cortex and hippocampus. Proc Natl Acad Sci USA. 103: 1071–1076.

Chen Y, Huang WC, Sejourne J, Clipperton-Allen AE, Page DT. 2015. Pten mutations alter brain growth trajectory and allocation of cell types through elevated beta-catenin signaling. J Neurosci. 35:10252–10267.

Dahlhaus M, Hermans JM, Van Woerden LH, Saiepour MH, Nakazawa K, Mansvelder HD, Heimel JA, Levelt CN. 2008. Notch1 signaling in pyramidal neurons regulates synaptic connectivity and experience-dependent modifications of acuity in the visual cortex. J Neurosci. 28:10794–10802.

Dahlhaus M, Li KW, Van der Schors RC, Saiepour MH, van NP, Heimel JA, Hermans JM, Loos M, Smit AB, Levelt CN. 2011. The synaptic proteome during development and plasticity of the mouse visual cortex. Mol Cell Proteomics. 10(5):M110. 005413. doi: 10.1074/mcp.M110.005413.

Danielson E, Zhang N, Metallo J, Kaleka K, Shin SM, Gerges N, Lee SH. 2012. S-SCAM/MAGI-2 is an essential synaptic scaffolding molecule for the GluA2-containing maintenance pool of AMPA receptors. J Neurosci. 32:6967–6980.

Drees F, Pokutta S, Yamada S, Nelson WJ, Weis WI. 2005. Alpha-catenin is a molecular switch that binds E-cadherin-beta-catenin and regulates actin-filament assembly. Cell. 123: 903–915.

Fox K, Sato H, Daw N. 1989. The location and function of NMDA receptors in cat and kitten visual cortex. J Neurosci. 9: 2443–2454.

Fox K, Sato H, Daw N. 1990. The effect of varying stimulus intensity on NMDA-receptor activity in cat visual cortex. J Neurophysiol. 64:1413–1428.

Goda Y. 2002. Cadherins communicate structural plasticity of presynaptic and postsynaptic terminals. Neuron. 35:1–3.

Heimel JA, Hartman RJ, Hermans JM, Levelt CN. 2007. Screening mouse vision with intrinsic signal optical imaging. Eur J Neurosci. 25:795–804.

Heimel JA, Saiepour MH, Chakravarthy S, Hermans JM, Levelt CN. 2010. Contrast gain control and cortical TrkB signaling shape visual acuity. Nat Neurosci. 13:642–648.

Hensch TK, Gordon JA, Brandon EP, McKnight GS, Idzerda RL, Stryker MP. 1998. Comparison of plasticity in vivo and in vitro in the developing visual cortex of normal and protein kinase A RIbeta-deficient mice. J Neurosci. 18:2108–2117.

Junghans D, Hack I, Frotscher M, Taylor V, Kemler R. 2005. Beta-catenin-mediated cell-adhesion is vital for embryonic forebrain development. Dev Dyn. 233:528–539.

Kamphuis W, Middeldorp J, Kooijman L, Sluijs JA, Kooi EJ, Moeton M, Freriks M, Mizee MR, Hol EM. 2014. Glial fibrillary acidic protein isoform expression in plaque related astrogliosis in Alzheimer's disease. Neurobiol Aging. 35:492–510.

Kleinschmidt A, Bear MF, Singer W. 1987. Blockade of "NMDA" receptors disrupts experience-dependent plasticity of kitten striate cortex. Science. 238:355–358.

Krumm N, O'Roak BJ, Shendure J, Eichler EE. 2014. A de novo convergence of autism genetics and molecular neuroscience. Trends Neurosci. 37:95–105.

Kwon HB, Kozorovitskiy Y, Oh WJ, Peixoto RT, Akhtar N, Saulnier JL, Gu C, Sabatini BL. 2012. Neuroligin-1-dependent competition regulates cortical synaptogenesis and synapse number. Nat Neurosci. 15:1667–1674.

Lee EJ, Choi SY, Kim E. 2015. NMDA receptor dysfunction in autism spectrum disorders. Curr Opin Pharmacol. 20:8–13.

Maguschak KA, Ressler KJ. 2008. Beta-catenin is required for memory consolidation. Nat Neurosci. 11:1319–1326.

Mao Y, Ge X, Frank CL, Madison JM, Koehler AN, Doud MK, Tassa C, Berry EM, Soda T, Singh KK, et al. 2009. Disrupted in schizophrenia 1 regulates neuronal progenitor proliferation via modulation of GSK3beta/beta-catenin signaling. Cell. 136:1017–1031.

Miller KD, Chapman B, Stryker MP. 1989. Visual responses in adult cat visual cortex depend on N-methyl-D-aspartate receptors. Proc Natl Acad Sci USA. 86:5183–5187.

Mills F, Bartlett TE, Dissing-Olesen L, Wisniewska MB, Kuznicki J, Macvicar BA, Wang YT, Bamji SX. 2014. Cognitive flexibility and long-term depression (LTD) are impaired following beta-catenin stabilization in vivo. Proc Natl Acad Sci USA. 111: 8631–8636.

Murase S, Mosser E, Schuman EM. 2002. Depolarization drives beta-Catenin into neuronal spines promoting changes in synaptic structure and function. Neuron. 35:91–105.

Nishimura W, Yao I, Iida J, Tanaka N, Hata Y. 2002. Interaction of synaptic scaffolding molecule and Beta -catenin. J Neurosci. 22:757–765.

Nuriya M, Huganir RL. 2006. Regulation of AMPA receptor trafficking by N-cadherin. J Neurochem. 97:652–661.

O'Roak BJ, Vives L, Girirajan S, Karakoc E, Krumm N, Coe BP, Levy R, Ko A, Lee C, Smith JD, et al. 2012. Sporadic autism exomes reveal a highly interconnected protein network of de novo mutations. Nature. 485:246–250.

Ochs SM, Dorostkar MM, Aramuni G, Schon C, Filser S, Poschl J, Kremer A, Van LF, Ovsepian SV, Herms J. 2015. Loss of neuronal GSK3beta reduces dendritic spine stability and attenuates excitatory synaptic transmission via beta-catenin. Mol Psychiatry. 20:482–489.

Okamura K, Tanaka H, Yagita Y, Saeki Y, Taguchi A, Hiraoka Y, Zeng LH, Colman DR, Miki N. 2004. Cadherin activity is required for activity-induced spine remodeling. J Cell Biol. 167:961–972.

Okuda T, Yu LM, Cingolani LA, Kemler R, Goda Y. 2007. beta-Catenin regulates excitatory postsynaptic strength at hippocampal synapses. Proc Natl Acad Sci USA. 104: 13479–13484.

Ozawa M, Baribault H, Kemler R. 1989. The cytoplasmic domain of the cell adhesion molecule uvomorulin associates with three independent proteins structurally related in different species. EMBO J. 8:1711–1717.

Pei F, Baldassi S, Norcia AM. 2014. Electrophysiological measures of low-level vision reveal spatial processing deficits and hemispheric asymmetry in autism spectrum disorder. J Vis. 14(11). pii: 3. doi: 10.1167/14.11.3.

Peng YR, He S, Marie H, Zeng SY, Ma J, Tan ZJ, Lee SY, Malenka RC, Yu X. 2009. Coordinated changes in dendritic arborization and synaptic strength during neural circuit development. Neuron. 61:71–84.

Pozza MF, Olpe HR, Brugger F, Fagg GE. 1990. Electrophysiological characterization of a novel potent and orally active NMDA receptor antagonist: CGP 37849 and its ethylester CGP 39551. Eur J Pharmacol. 182:91–100.

Saiepour MH, Chakravarthy S, Min R, Levelt CN. 2015. Competition and Homeostasis of Excitatory and Inhibitory Connectivity in the Adult Mouse Visual Cortex. Cereb Cortex. 25:3713–3722.

Sato M, Stryker MP. 2008. Distinctive features of adult ocular dominance plasticity. J Neurosci. 28:10278–10286.

Sawtell NB, Frenkel MY, Philpot BD, Nakazawa K, Tonegawa S, Bear MF. 2003. NMDA receptor-dependent ocular dominance plasticity in adult visual cortex. Neuron. 38:977–985.

Schuman EM, Murase S. 2003. Cadherins and synaptic plasticity: activity-dependent cyclin-dependent kinase 5 regulation of synaptic beta-catenin-cadherin interactions. Philos Trans R Soc Lond B Biol Sci. 358:749–756.

Self MW, Kooijmans RN, Super H, Lamme VA, Roelfsema PR. 2012. Different glutamate receptors convey feedforward and recurrent processing in macaque V1. Proc Natl Acad Sci USA. 109:11031–11036.

Sun Y, Aiga M, Yoshida E, Humbert PO, Bamji SX. 2009. Scribble interacts with beta-catenin to localize synaptic vesicles to synapses. Mol Biol Cell. 20:3390–3400.

Tai CY, Mysore SP, Chiu C, Schuman EM. 2007. Activity-regulated N-cadherin endocytosis. Neuron. 54:771–785.

Tang L, Hung CP, Schuman EM. 1998. A role for the cadherin family of cell adhesion molecules in hippocampal long-term potentiation. Neuron. 20:1165–1175.

Tapia M, Del PA, Puime A, Sanchez-Ponce D, Fronzaroli-Molinieres L, Pallas-Bazarra N, Carlier E, Giraud P, Debanne D, Wandosell F, et al. 2013. GSK3 and beta-catenin determines functional expression of sodium channels at the axon initial segment. Cell Mol Life Sci. 70:105–120.

Togashi H, Abe K, Mizoguchi A, Takaoka K, Chisaka O, Takeichi M. 2002. Cadherin regulates dendritic spine morphogenesis. Neuron. 35:77–89.

Tsumoto T. 1990. Excitatory amino acid transmitters and their receptors in neural circuits of the cerebral neocortex. Neurosci Res. 9:79–102.

Tsumoto T, Hagihara K, Sato H, Hata Y. 1987. NMDA receptors in the visual cortex of young kittens are more effective than those of adult cats. Nature. 327:513–514.

Tsumoto T, Masui H, Sato H. 1986. Excitatory amino acid transmitters in neuronal circuits of the cat visual cortex. J Neurophysiol. 55:469–483.

Tucci V, Kleefstra T, Hardy A, Heise I, Maggi S, Willemsen MH, Hilton H, Esapa C, Simon M, Buenavista MT, et al. 2014. Dominant beta-catenin mutations cause intellectual disability with recognizable syndromic features. J Clin Invest. 124:1468–1482.

Tyler CW, Apkarian P, Levi DM, Nakayama K. 1979. Rapid assessment of visual function: an electronic sweep technique for the pattern visual evoked potential. Invest Ophthalmol Vis Sci. 18:703–713.

Vitureira N, Letellier M, White IJ, Goda Y. 2012. Differential control of presynaptic efficacy by postsynaptic N-cadherin and beta-catenin. Nat Neurosci. 15:81–89.

Weinger PM, Zemon V, Soorya L, Gordon J. 2014. Low-contrast response deficits and increased neural noise in children with autism spectrum disorder. Neuropsychologia. 63:10–18.

Wickline ED, Awuah PK, Behari J, Ross M, Stolz DB, Monga SP. 2011. Hepatocyte gamma-catenin compensates for conditionally deleted beta-catenin at adherens junctions. J Hepatol. 55:1256–1262.

Yamada S, Pokutta S, Drees F, Weis WI, Nelson WJ. 2005. Deconstructing the cadherin-catenin-actin complex. Cell. 123:889–901.